Nature Climate Change
October 2023, Volume 13 Issue 10 Pages 1114–1121
https://doi.org/10.1038/s41558-023-01790-6
https://archimer.ifremer.fr/doc/00942/105393/

Marine biodiversity exposed to prolonged and intense subsurface heatwaves

Fragkopoulou Eliza [1? *], Sen Gupta Alex [2, 3], Costello Mark John [4], Wernberg Thomas [5, 6], Araújo Miguel B. [7, 8], Serrão Ester A. [1], De Clerck Olivier [9], Assis Jorge [1, 4, *]

[1] CCMAR – Centre of Marine Sciences, University of Algarve, Faro, Portugal
[2] Climate Change Research Centre, University of New South Wales, Sydney, New South Wales, Australia
[3] Australian Research Council Centre of Excellence for Climate Extremes, University of New South Wales, Sydney, New South Wales, Australia
[4] Faculty of Biosciences and Aquaculture, Bodø, Norway
[5] UWA Oceans Institute & School of Biological Sciences, University of Western Australia, Crawley, Western Australia, Australia
[6] Norwegian Institute of Marine Research, Flødevigen Research Station, His, Norway
[7] Department of Biogeography and Global Change, National Museum of Natural Sciences, CSIC, Madrid, Spain
[8] Rui Nabeiro Biodiversity Chair, MED – Mediterranean Institute for Agriculture, Environment and Development, University of Évora, Évora, Portugal
[9] Phycology Research Group, Biology Department, Ghent University, Ghent, Belgium

* Corresponding authors : Eliza Fragkopoulou, email address : eli_frag@hotmail.com ; Jorge Assis, email address : jorgemfa@gmail.com

Abstract :

Marine heatwaves (MHWs) are becoming increasingly common, with devastating ecosystem impacts. However, MHW understanding has almost exclusively relied on sea surface temperature with limited knowledge about their subsurface characteristics. Here we estimate global MHWs from the surface to 2,000 m depth, covering the period 1993–2019, and explore biodiversity exposure to their effects. We find that MHWs are typically more intense in the subsurface at 50–200 m and their duration increases up to twofold with depth, although with large spatial variability linked to different oceanographic conditions. Cumulative intensity (a thermal stress proxy) was highest in the upper 250 m, exposing subsurface biodiversity to MHW effects. This can be particularly concerning for up to 22% of the ocean, where high cumulative intensity overlapped the warm range edge of species distributions, thus being more sensitive to thermal stress. Subsurface MHWs can hence drive biodiversity patterns, with consequent effects on ecological interactions and ecosystem processes.

Keywords : Biodiversity, Marine biology, Physical oceanography

Main

The frequency and duration of marine heatwaves (MHWs) have been increasing over the past century[1–3] and are anticipated to further increase in the decades to come[4], driven by anthropogenic climate change and ocean warming[1,2,5]. MHWs have caused substantial biological[6,7] and socio-ecological[8] impacts globally, ranging from rapid shifts in species distributions to mass mortality of marine organisms[8–10]. To date, MHWs have been studied primarily at the ocean surface due to the availability of high-quality sea surface temperature datasets[9] and only a few studies, all based on individual locations or events, have examined MHWs throughout the water column[10–18]. These studies focused on sites with long-term mooring data[16,17], or individual strong long-lasting MHWs partially resolved using ARGO data[11,13,14], or ocean models[12,15,18]. A global assessment of MHW spatial and temporal depth structure is still missing, hindering the examination of commonalities and differences across regions.

Localised observations have shown greater MHW intensity in the subsurface[11,13,16,17], with warming persisting for up to 2 years after the end of surface events[19]. Several processes can affect the depth structure of MHWs. In the north-eastern Pacific, salinity differences impacting the water column stratification determined the depth extent of warming during two distinct MHW events[13]. The enhanced stratification in 2019-2020 restricted the warming from extending as deep as in the 2013-2016 event[13]. In the tropical western Pacific, subsurface MHWs were related to Ekman convergence and downwelling of warm surface waters[17]. In south-eastern Australia, local downwelling also caused subsurface warming, at times without a surface signal[11,16]. In the north-western Atlantic, subsurface MHWs were driven by warm core rings spinning off the Gulf Stream boundary current over the slope and shelf region and were decoupled from surface events[18].

Given that MHW intensity may be stronger below the surface[11,13,16,17], a global characterization of subsurface MHWs could improve understanding of their potential impacts on marine biodiversity[9,20]. Here, we advance this understanding by using global high-resolution (1/12º) reanalysis temperature data[21] from 1993-2019 at eleven depths (0, 25, 50, 75, 100, 150, 200, 250, 500, 1000 and 2000 m), validated against *in-situ* observations (S1), to estimate MHW metrics per depth and over time. Further, we provide novel insights into the potential biodiversity exposure to MHWs globally by overlaying the spatial distribution of cumulative MHW intensity with species richness estimates[22] derived from the modelled ranges of 25,078 species distributed from the surface to 2000 m[23].

Global MHW metrics with depth

Temperature reanalysis data from 1993 to 2019 showed multi-decadal warming of the global ocean, with a stronger signal above 500 m (Fig. 1a). In the upper 100 m, warming was modulated by strong interannual variability, such as the extreme 1997/98 and 2016/17 El Niño events[24], whose impacts become lagged with depth. The progressive warming of the global ocean expanded in depth, reaching 1000 m over recent years, with a lack of cold temperature anomalies after 2015 (Fig.1a). The reanalysis and *in-situ* data showed a good agreement (S1 Table 2), yet temperature estimates from the deep ocean, polar latitudes, ice-covered regions and prior to 2004, when subsurface ARGO float data measurements were less widespread, should be interpreted with caution because they are highly uncertain (see methods).

The global average MHW maximum intensity, that is the average of the maximum temperature anomaly from the climatology of each MHW event, remained greater than 1.3°C in the upper 200 m of the ocean (Fig. 1). Remarkably, the highest intensity was found at 100 m depth with a mean ± SD of 1.6 ± 1.0°C. This was 19% higher than surface events (1.3 ± 0.5°C; Fig. 1; S2 Table 1). Even at 200 m depth, the intensity was still as high as at the surface (1.3 ± 0.8°C). Deeper than 200 m, global MHW intensity typically reduced with depth, decreasing to 0.37 ± 0.28°C at 1000 m and 0.15 ± 0.09°C at 2000 m depth (Fig. 1; S2 Table 1). This global pattern of subsurface MHW intensification could be related to vertical displacements of the thermocline, the upper ocean layer characterized by a steep temperature gradient with depth (Fig. 1f), resulting in warmer temperatures at fixed depths[11,13,16,17].

The globally averaged occurrence of MHWs (i.e., the number of individual events from 1993 to 2019) decreased with depth, from an average of 44 ± 10 events at the surface to 28 ± 11 events at 2000 m depth (Fig. 1; S2 Table 1). Conversely, the average duration of MHW increased two-fold, from 20 ± 6 days at the surface to 40 ± 19 days at 2000 m depth (Fig. 1; S2 Table 1). Notably, both metrics showed little variation between 50 and 250 m depth.

The sum of cumulative intensity, i.e., the integral of MHW intensity over the duration of each event[25] (in degree days; Fig. 1e), was estimated as a proxy of thermal stress. This ranged from an average of 1007 ± 435 degree-days at the surface to 141 ± 92 degree-days at 2000 m (S2 Table 1). Like the intensity pattern, the highest average cumulative intensity was at 100 m depth with a mean of 1439 ± 849 degree-days. At 500 m, MHW cumulative intensity decreased to almost half than at the surface and continued to decrease in deeper waters, despite the increase in MHW duration (Fig. 1; S2 Table 1).

Timeseries analyses of temperature anomalies revealed strong synchrony between surface and subsurface layers down to 50 m depth (corr. 0.75 ± 0.24; S2 Table 1), decreasing rapidly from the surface to 100 m and more slowly subsequently, yet with large variability (Fig. 1g). The increased synchrony in the upper 100 m is to be expected, as this represents the typical mixed layer depth within which water mass homogenization occurs[26]. Below the mixed layer, reduced synchrony in warming indicates disassociated processes of surface and subsurface temperature variability and therefore potentially disassociated MHW drivers.

Spatial patterns of MHWs

Spatial variations in MHW metrics prevailed across depths (Fig. 2). The strongest and most frequent MHWs were primarily observed in regions of sharp temperature gradients, such as those associated with boundary currents and fronts. However, these events tended to have a short duration (Fig. 2). For example, in the Gulf Stream (north-western Atlantic Ocean) and Agulhas Current (south Indian Ocean) extensions, frequent and strong MHWs were detected as deep as 1000 m (Fig. 2), matching the depth extension of the boundary currents[27]. Strong MHWs also occurred in regions along the equator but in the subsurface (e.g., 100 m depth; Fig. 2). The longest MHW durations were often estimated in polar regions (e.g., Weddell Sea in the Antarctic), a pattern that was replicated down to the maximum depth (Fig. 2). At 2000 m, prolonged MHWs were common in every ocean basin (Fig. 2).

Biodiversity exposure to MHWs

We used MHW cumulative intensity (degree-days) and species distributions to estimate biodiversity exposure to MHWs. In this context, we defined richness exposure as the overlap of cumulative intensity and species richness[22] (i.e., the number of species in each cell; Fig. 3). Because thermal tolerances are more easily exceeded at the warm range edge of species distributions[6], we used warm-edge exposure as a proxy of thermal sensitivity and define it as the overlap of cumulative intensity and warm-edge richness (i.e., the number of species at the warm range edge of their distributions in each cell; Fig. 3, S1 Fig. 8). Regions of highest/least exposure were defined where high richness overlayed high/low cumulative intensity.

Overall, regions of highest richness exposure varied across depths (Fig. 3), depending on MHW cumulative intensity and species richness estimates, with both being greater in the upper 250 m of the ocean (S2 Table 2). Averaged across depths, 14% of the ocean was classified as high richness exposure, ranging between 11% at the surface and 250 m depth and 16% at 75 and 100 m depth (Fig. 3; S2 Table 2). Despite spatial variability, some regions were recurrently classified as high richness exposed across depths, such as in the Philippine and Tasman Seas (West Pacific), the Gulf of Mexico (North Atlantic) and off South Africa in the South Indian Ocean. In contrast, regions of least richness exposure represented a smaller portion of the ocean (8% on average), ranging between 6% (e.g., equatorial Pacific at 500 m depth) and 11% (e.g., surface tropical Atlantic). Highest warm-edge exposure comprised an average of 15% of the global ocean across depths, ranging from only 6% at the surface to up to 22% at 1000-2000 m depth, comprising large portions of the Indian and North Atlantic Oceans (Fig. 3; S2 Table 3). Regions such as the Gulf of Mexico, the Gulf of Aden and the Tasman Sea were consistently classified as highly exposed across depths, both for richness and warm-edge exposure, being of particular concern for potential biological effects. In contrast, regions classified as least warm-edge exposed represented on average 8% of the ocean, ranging from 3% at 500 m (e.g., North Indian Ocean) to 17% at the surface (e.g., tropical Atlantic and Indian oceans; Fig. 3; S2 Table 3).

Local MHW and biodiversity patterns

Local time-depth analyses of maximum MHW intensity and biodiversity metrics were produced for selected locations with distinct oceanographic or climatic conditions. Different patterns in the intensity, frequency, duration and depth extent of MHW events emerged, depending on the prevailing conditions (Fig. 4; Extended Data Fig. 1; Extended Data Fig. 2). In regions of boundary currents and fronts (Fig. 4a,b; Extended Data Fig. 1a,b), MHWs typically extended at depths well below the thermocline, reaching down to 1000 m (S1 Fig. 9ab). Under these conditions, MHWs had a short duration, and the highest (cumulative) intensity was typically found from the surface to 500 m depth. In regions of subtropical gyres (Fig. 4c; Extended Data Fig. 2c), MHWs tended to last longer, and higher MHW (cumulative) intensities were found from the surface to the thermocline depth (S1 Fig. 9c), where they often peaked. Weaker intensity MHWs also occurred below the thermocline, at times unconnected to surface events. In regions of tropical gyres (Fig. 4d; Extended Data Fig 2d), subsurface MHWs were predominantly unconnected to the surface and had shorter durations. The highest intensities were estimated in the subsurface at the thermocline depth (S1 Fig. 9d). In the Arctic (Fig. 4e; Extended Data Fig. 2e), subsurface MHWs were particularly prolonged (up to 3 years) and appeared to be mostly unconnected to the surface. They primarily occurred below the thermocline depth (S1 Fig. 9e), where cumulative intensity peaked despite the higher intensities found at the surface. Regional biodiversity patterns of species and warm-edge richness varied greatly among regions and depths, ranging from over 400 species richness in the subtropical South Atlantic to less than 10 in the Arctic, with a richness increase in deeper demersal communities (Fig. 4; Extended Data Fig. 2). The highest exposure to MHW effects, estimated in depths where richness and cumulative intensity were the greatest, was between 50-100 m depth across all regions except for boundary currents, where exposure peaked deeper, at 250-500 m.

Discussion

Using state-of-the-art reanalysis data, we show that globally subsurface MHWs are, on average, longer and more intense than surface events, with up to 22% of the subsurface ocean being in the highest biodiversity exposure category. Biodiversity impacts could be greater in the upper 250 m of the ocean, where MHW (cumulative) intensity was the highest. This can be particularly concerning at the warm range edge of species' distribution, where thermal tolerances are easily exceeded and more impacts have been recorded[6,7]. Thus, potential depth and distribution range shifts are likely in the upper 250 m as a response to acute warming, driving changes in global biodiversity patterns with consequent effects on marine communities and ecological interactions[28,29]. However, the large variability found in the regional patterns of MHWs highlights a complex picture of biodiversity exposure across depths and regions.

Our results are consistent with previous regional findings[10–18] and show that strong subsurface MHWs are conspicuous across the global ocean, with varying characteristics that depend on the prevailing oceanographic conditions. Surface events often extended to a considerable depth, particularly in regions of boundary currents and oceanographic fronts (Fig. 4a,b), but subsurface MHWs still occurred without a surface signal, driven by distinct mechanisms (Fig. 4c,d,e). MHW duration increased with depth across the ocean, yet the most prolonged events were often estimated in the subsurface of polar regions (Fig. 2). Despite the acknowledged uncertainties of polar estimates (see methods), additional studies corroborate the trends in our findings. The long-lasting subsurface MHWs in the Arctic Ocean are in line with its borealization by Atlantic[30] and Pacific[31] warm subsurface water flows at ~150-900 m depth. Similar trends of subsurface warming have been reported across the Antarctic[32], including the Weddell Sea[33], where we estimated long-lasting subsurface MHWs.

The spatial variation in MHW characteristics is suggestive of distinct driving mechanisms for different MHW types: the surface-confined, those that are intensified in the subsurface, or that do not have a surface expression and those extending below the surface mixed layer (Fig. 4). Events confined to the mixed layer (e.g., Fig. 4c; S1 Fig. 9c) are likely generated by surface drivers, such as surface currents[9,34,35] or anomalies in air-sea heat fluxes[34,35]. Yet, their depth extension may depend on the stratification of the water column (S1 Fig. 9c), with weak stratification linked to deeper warming[11,13,14,16,17]. Changes in seasonal timing (e.g., the beginning of monsoon season) can influence the background variability of the ocean (e.g., salinity and thermocline depth), thereby affecting the probability of subsurface MHW emergence, without a surface signal (e.g., Fig. 4d)[10–17]. Specifically, changes in wind patterns can prevent MHW emergence through upwelling[36] or promote it through Ekman downwelling, driving subsurface MHWs below the mixed layer (S1 Fig. 9c,d), where warming is insulated from surface processes and therefore can last longer[10–12,14–17]. Rossby and equatorial Kelvin waves can also drive changes in the climate and circulation conditions, influencing the emergence of subsurface MHWs around the thermocline[17,37]. At boundary currents and fronts (Fig. 4a,b), MHWs can extend hundreds of meters into the water column, well below the thermocline depth (S1 Fig. 9a,b), driven by anomalous current circulation[11,12,14,15,17,18], related to variations in their location, strength and heat content.

Distinguishing the mechanisms driving each MHW event is challenging due to limited large-scale, long-term oceanographic and atmospheric data, as multiple, complex drivers can interact favouring or preventing MHW emergence. Therefore, systematic monitoring of the global ocean across depths is necessary to enable a better understanding of subsurface MHW drivers and potential changes related to future climate change.

MHWs have caused abrupt ecosystem changes across the globe, triggering diverse ecophysiological responses of marine organisms[38–40]. Most responses have been reported from shallow coastal regions (< 40 m[41]), however, we show high MHW (cumulative) intensities in the upper 250 m, translated into increased biodiversity exposure at depths depending on the oceanographic conditions (e.g., at 50-100 m in tropical gyres and 250-500 m in boundary currents). Coastal ecosystems, being readily accessible, are more frequently monitored and biodiversity responses of deeper ecosystems could be overlooked. Indeed, deep surveys have reported MHWs impacts extending to mesopelagic reefs, down to 100 m depth[42–44]. MHW impacts can be particularly detrimental on warm range edge populations of sessile species[6,7], whose individuals cannot move to cooler waters. Characteristic examples include the coral bleaching in the Great Barrier Reef[45] and the extensive kelp forest losses in southern Australia and the north-eastern Pacific[46,47]. In regions where multiple species have their warm range edges (i.e., high warm-edge exposure), such as southwestern Australia and the coast of Alaska (Fig. 3), MHW effects can be magnified into entire community shifts, lasting for years after the events[38,39]. As MHWs become more frequent/intense under long-term warming[4], species depth ranges are expected to deepen[48] and may become vertically compressed[49], as already reported for cold-water species in the Mediterranean Sea[28]. However, where strong internal temperature variability prevails, such as in current fronts like the Gulf Stream or at thermoclines like those of tropical gyres (Fig. 4a,d), populations may have adapted their physiological responses to local temperature conditions[50–53]. But despite species' plasticity, ecosystems can still suffer abrupt changes, especially when MHWs are frequent[54,55], prolonged[38] and coupled with additional disturbances[56,57].

Deeper than 250 m, MHWs are on average half as intense as at the surface (<1°C). Empirical evidence of ecophysiological responses to thermal stress is limited for these ecosystems, but available reports show temperature changes of only 0.1-0.4°C affecting species richness and community structure of nematodes at 1500 m depth[58] and peracarid crustaceans at depths of 600-2300 m[59]. This suggests that deep-sea biodiversity could be sensitive to small temperature changes. Despite the low intensities, MHWs in the deep ocean may still have implications for biodiversity, especially if coupled with declines in oxygen concentration, pH and organic material fluxes[60,61]. For example, despite the decrease in MHW cumulative intensity below 500 m depth, this depth coincides with oxygen minimum zones for vast regions of the ocean[61], therefore even a weak MHW could act synergistically on the response of the ecosystems. However, empirical evidence is needed to verify this hypothesis.

While most studies reporting the impact of extreme ocean temperatures on biodiversity are based on surface events, the high exposure found down to 250 m depth suggests that subsurface biodiversity is also at considerable risk. Previous work has shown that the main driver behind the increase in intensity and frequency of MHWs is ocean warming[5]. While ocean warming could be more near the surface, warming does persist in the deep ocean and is projected to increase in the future[62]. As such, future MHWs will likely become more frequent and intense across all depths further exposing biodiversity to their effects. This might shift species' depth distributions, particularly in the upper to 250 m of the ocean, potentially changing global biodiversity patterns with consequent effects on ecological interactions and ecosystem processes. However, these shifts may be hindered by low oxygen zones or the lack of species' physiological adaptations to the conditions of the deeper ocean[63]. Baseline empirical evidence and time-series analyses of deep-sea communities under MHWs are needed to acknowledge their response to warming and increased MHWs, as those may be going unnoticed.

Acknowledgements

This study received Portuguese national funds from FCT - Foundation for Science and Technology through the projects UIDB/04326/2020, UIDP/04326/2020, PTDC/BIA-CBI/6515/2020, LA/P/0101/2020 and DivRestore/013/2020 to EF, ES and JA, the Individual Call to Scientific Employment Stimulus 2022.00861 to JA and the fellowship SFRH/BD/144878/2019 to EF. A Pew Marine Fellowship to ES, funding from the Australian Research Council (DP200100201) to TW, an Australian Research Council Future Fellowship (FT220100475) to ASG and funding from BNP-PARIBAS Foundation, through the CORESCAM project ("Coastal Biodiversity Resilience to Increasing Extreme Events in Central America") to MBA. Lastly, the authors acknowledge the Copernicus Marine Environment Monitoring Service for proving the reanalysis data (https://data.marine.copernicus.eu/products).

Authors contributions

EF, JA and ODC conceived the study. EF and JA conducted the analyses. EF led the writing with the support of all authors. All authors revised the final draft and approved the submitted manuscript.

Competing interests

The authors declare no competing interests.

Figures

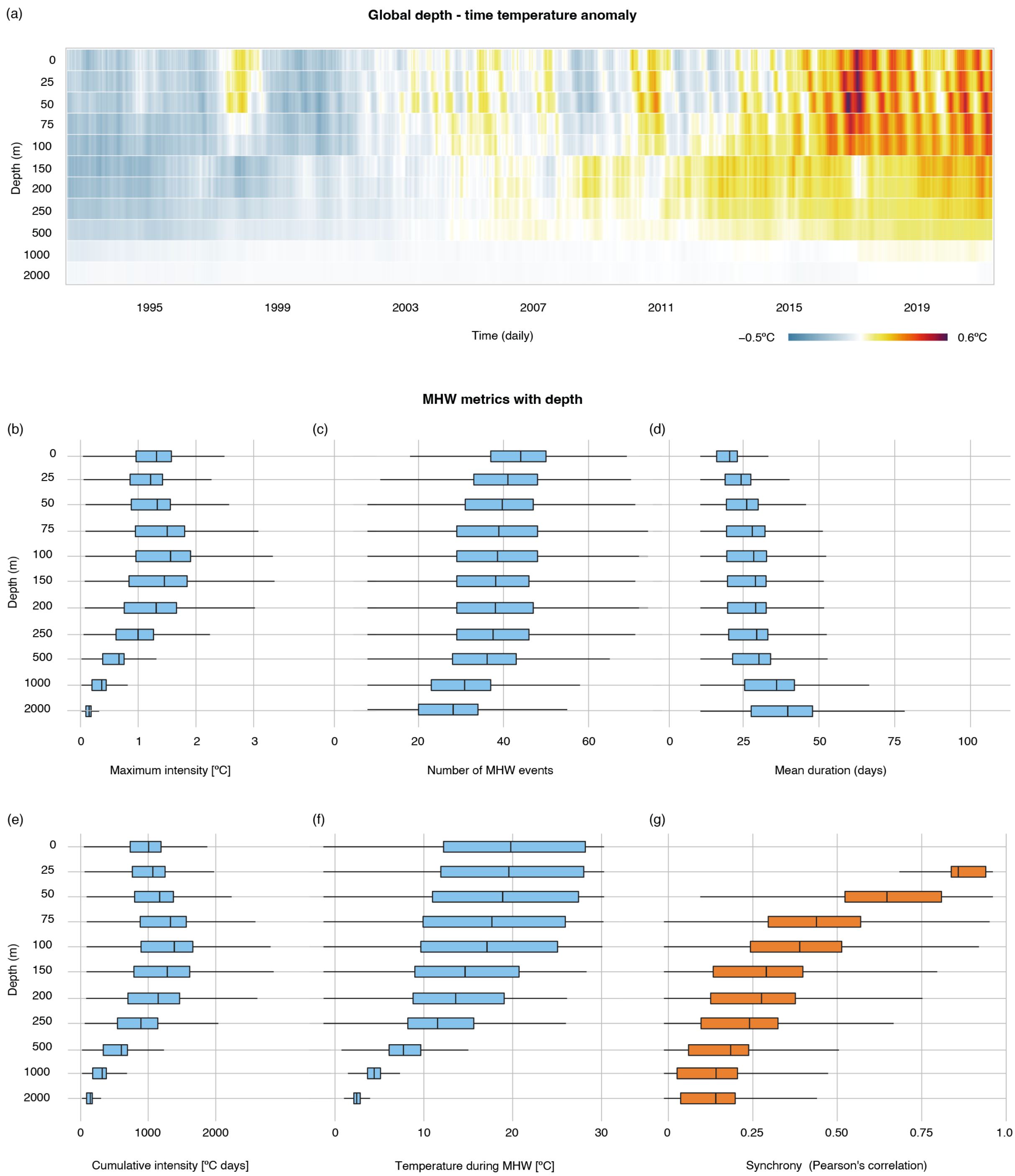

Fig. 1: Global marine heatwave (MHW) metrics from the surface to 2000 m for the period 1993-2019. **(a)** Time-depth global average temperature anomalies at each depth (levels not to scale). Global average estimates of MHW **(b)** maximum intensity, **(c)** occurrence, **(d)** duration, **(e)** cumulative intensity, and **(f)** ocean temperature during maximum MHW intensity, for each depth. **(g)** Temporal correlation of temperature anomalies between the surface and subsurface levels (95% confidence level). The boxplot central line represents the mean, edges the 25th and 75th percentile and whiskers the 5th and 95th percentile of values (n=31,073 cells). Outliers are not shown but full range values are presented in S2 Table 1.

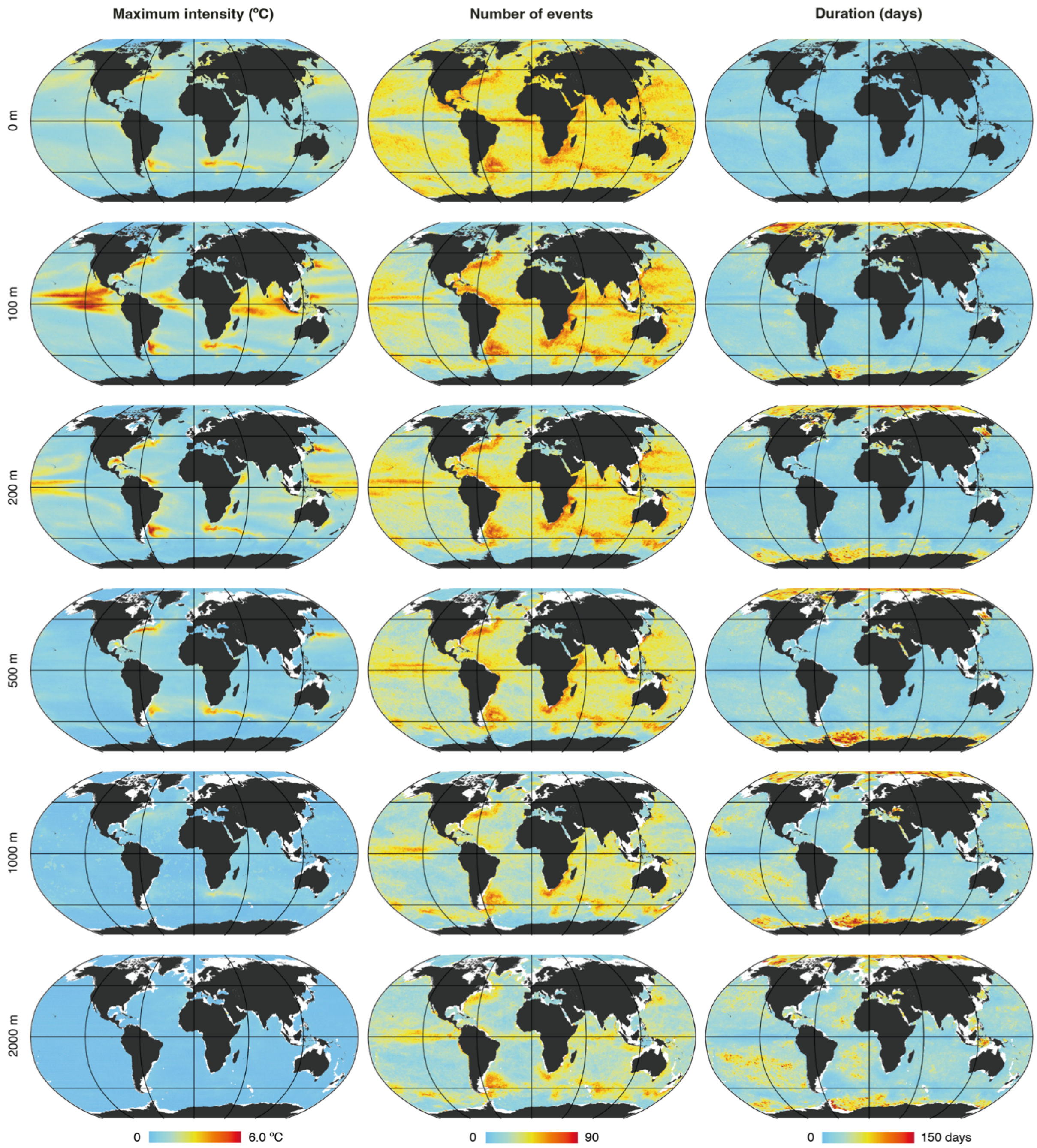

Fig. 2. Spatial distribution of marine heatwave (MHW) metrics with depth for the period 1993-2019. Global maps depicting MHW maximum intensity, occurrence (number of events from 1993 to 2019) and average duration. White map areas have no corresponding data because the ocean floor does not reach these depths. Maps are presented in Robinson projection with the main graticules depicted. Scales have been adapted to improve visibility; full ranges can be found in S2 Table 1.

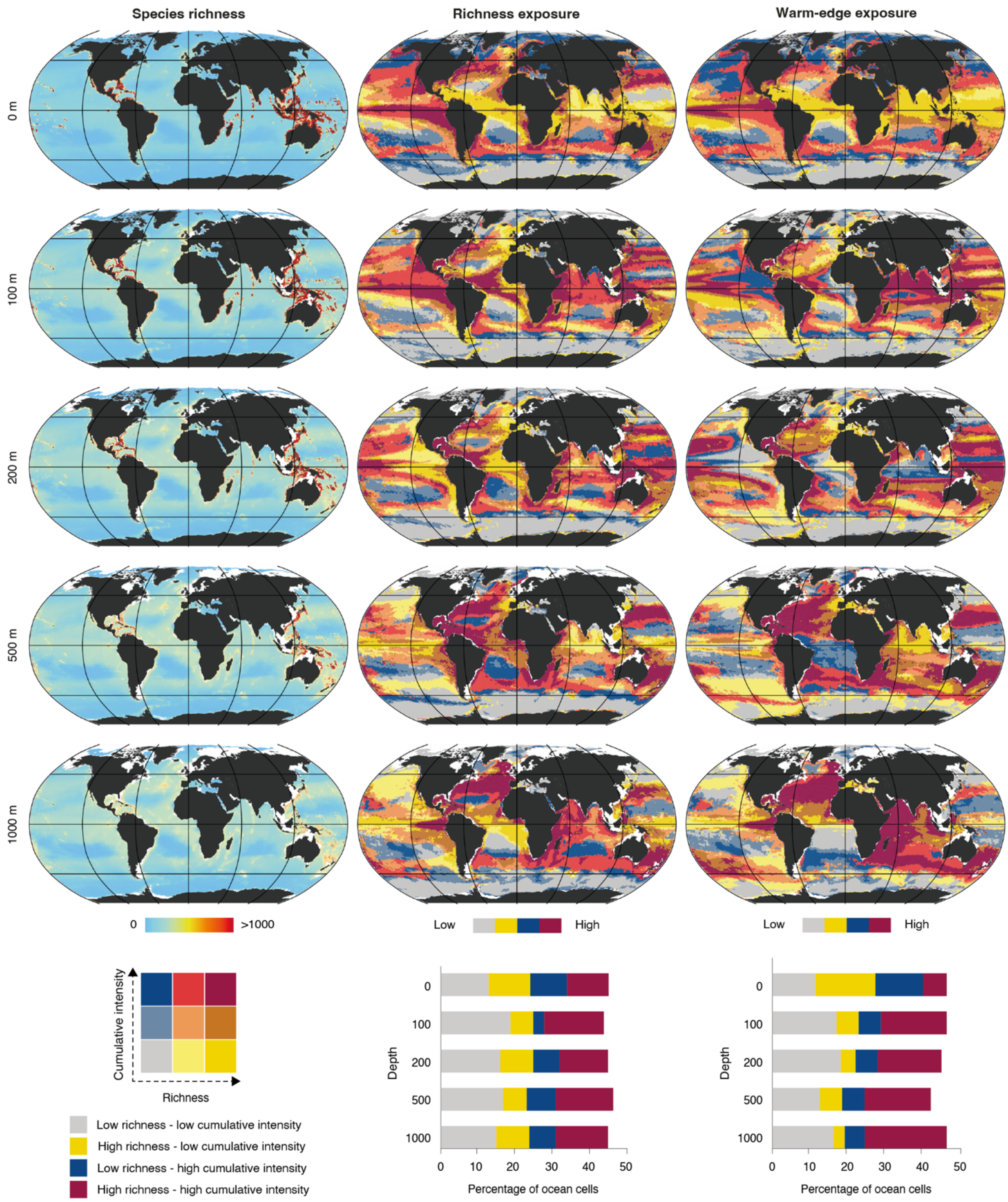

Fig. 3: Spatial distribution of biodiversity exposure to marine heatwaves (MHWs) with depth for the period 1993-2019. Global maps depicting species richness, richness exposure and warm-edge exposure to MHWs. Cumulative intensity, species richness and warm-edge richness were divided into terciles. Exposure was defined as the overlap of tercile combinations between cumulative intensity and biodiversity metrics, forming nine exposure categories. The percentage of ocean cells for the four most extreme overlapping terciles is

shown. White map areas have no corresponding data because the ocean floor does not reach these depths. Maps are presented in Robinson projection with the main graticules depicted.

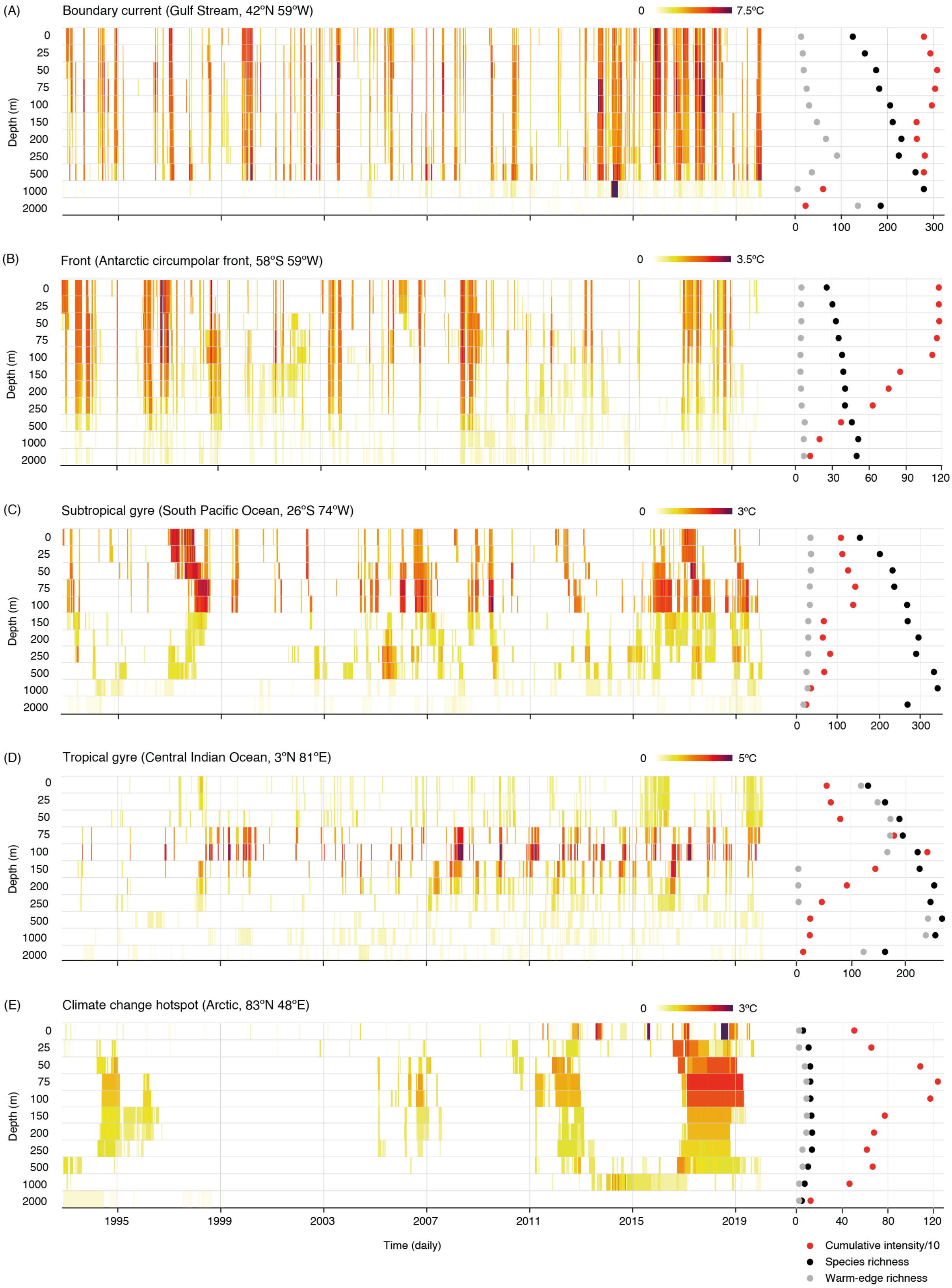

Fig. 4: Local marine heatwave (MHW) and biodiversity patterns in selected regions of distinct oceanographic or climatic conditions. Time-depth maximum MHW intensity, cumulative intensity, species and warm-edge richness for **(A)** boundary current, **(B)** oceanographic front, **(C)** subtropical and **(D)** tropical gyre, and **(E)** Arctic Ocean**.** Depth levels and temperature scales are not to scale. Regional characteristics were estimated from a 2 by 2-degree resolution cell. The geographic location of each offshore region and additional analyses of replicate regions are shown in Extended Data Fig. 1 and Extended Data Fig. 2.

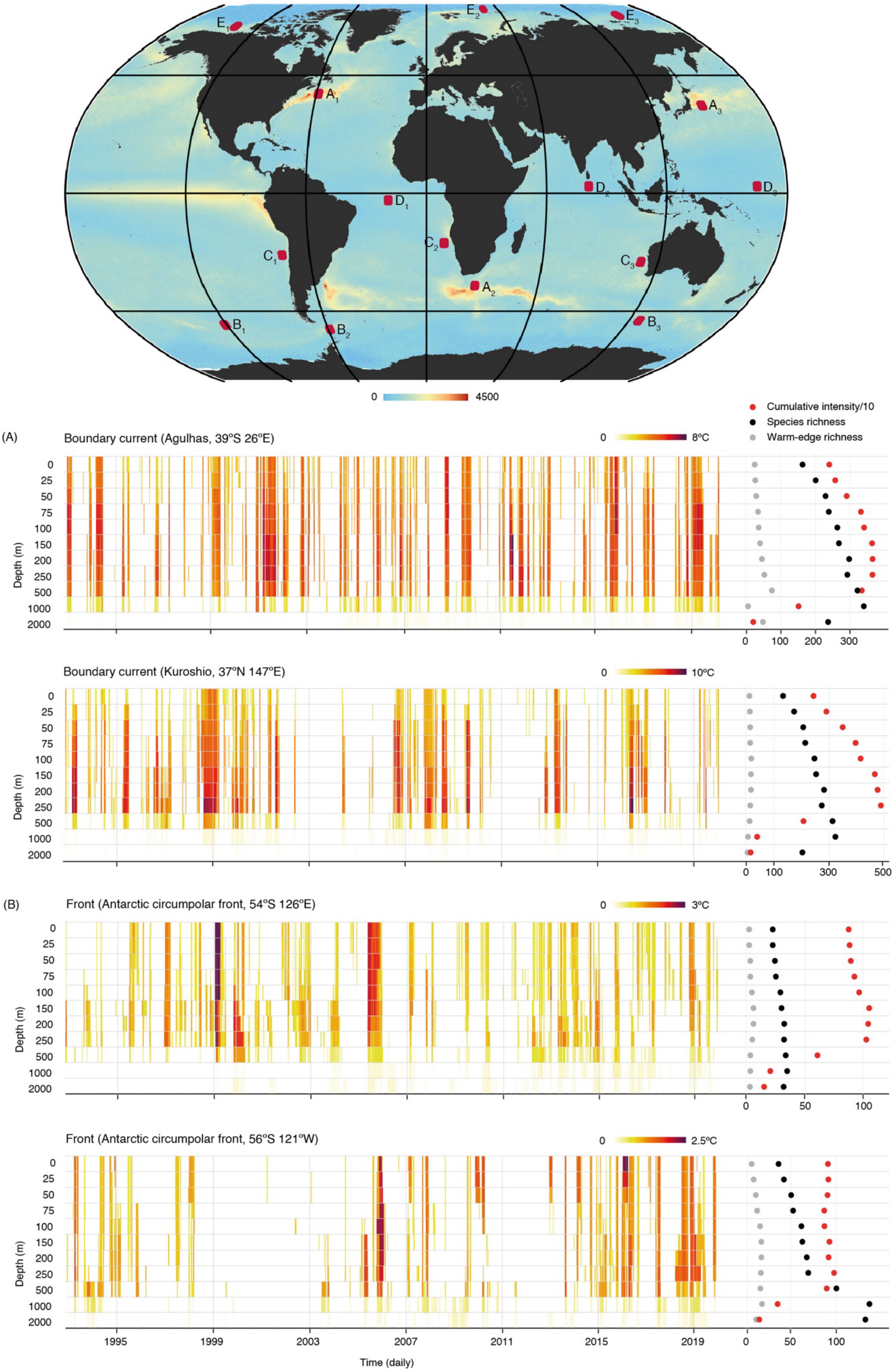

Extended Data Fig. 1: Local marine heatwave (MHW) and biodiversity patterns in selected regions of distinct oceanographic or climatic conditions. Global map depicting the geographic location of **(A)** boundary current, **(B)** oceanographic front, **(C)** subtropical and **(D)** tropical gyre, and **(E)** Arctic Ocean. Time-depth maximum MHW intensity, cumulative intensity, species and warm-edge richness are shown for regions of boundary current and oceanographic front (remaining regions are shown in Extended Data Fig. 2). Depth levels and temperature scales are not to scale. Regional characteristics were estimated from a 2 by 2-degree resolution cell. The global map features MHW cumulative intensity at the surface.

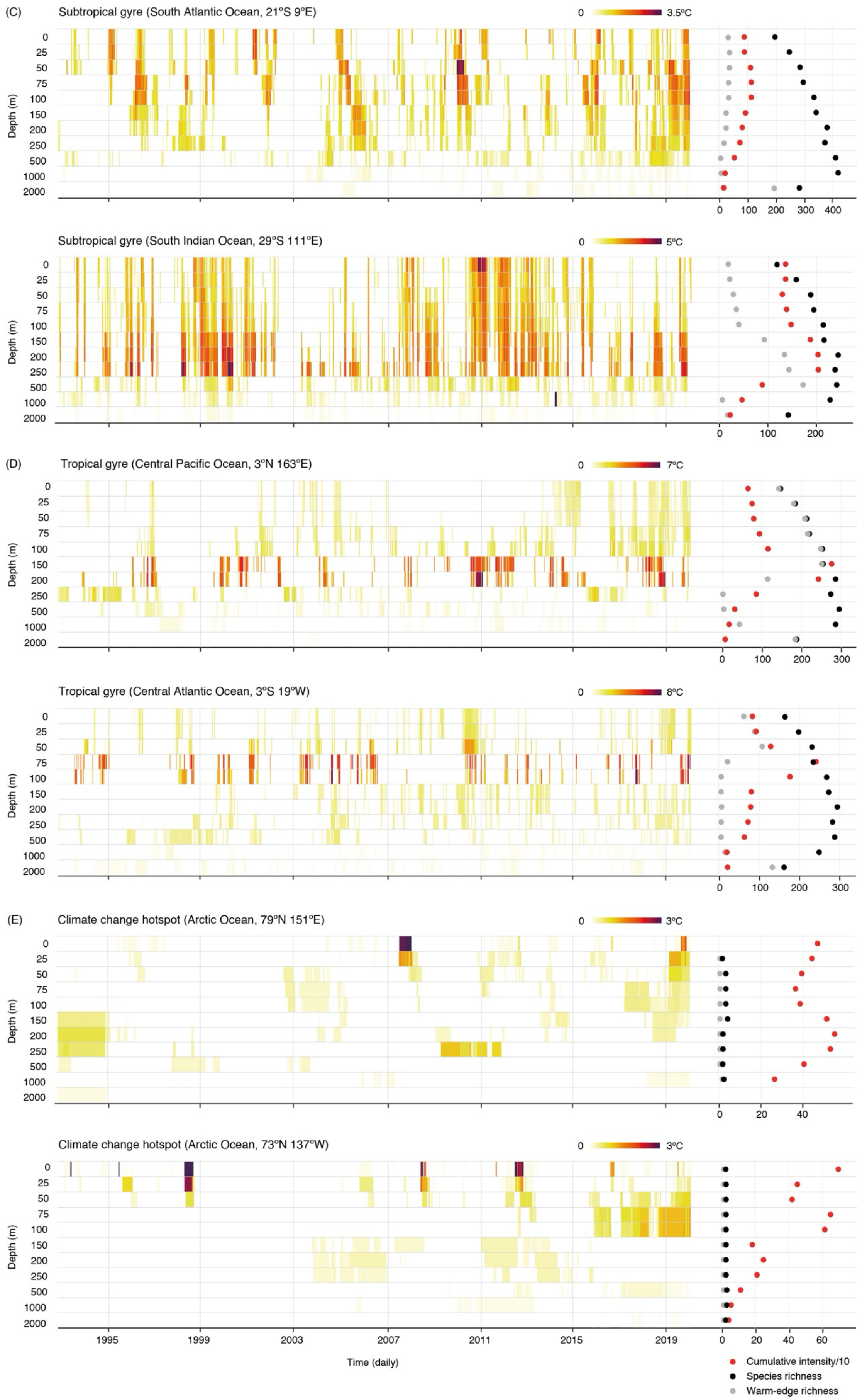

Extended Data Fig. 2: Local marine heatwave (MHW) and biodiversity patterns in selected regions of distinct oceanographic or climatic conditions. (Continuous from Extended Data Fig. 1) Time-depth maximum MHW intensity, cumulative intensity, species and warm-edge richness for regions of **(C)** subtropical and **(D)** tropical gyre, and **(E)** Arctic Ocean. Depth levels and temperature scales are not to scale. Regional characteristics were estimated from a 2 by 2-degree resolution cell. The geographic location of each region is depicted in the global map of Extended Data Fig. 1.

References

1. Frölicher, T. L., Fischer, E. M. & Gruber, N. Marine heatwaves under global warming. *Nature* **560**, 360–364 (2018).
2. Oliver, E. C. J. *et al.* Longer and more frequent marine heatwaves over the past century. *Nat Commun* **9**, 1324 (2018).
3. Tanaka, K. R. & van Houtan, K. S. The recent normalization of historical marine heat extremes. *PLOS Climate* **1**, e0000007 (2022).
4. Oliver, E. C. J. *et al.* Projected Marine Heatwaves in the 21st Century and the Potential for Ecological Impact. *Front Mar Sci* **6:734**, (2019).
5. Oliver, E. C. J. Mean warming not variability drives marine heatwave trends. *Clim Dyn* **53**, 1653–1659 (2019).
6. Smale, D. A. *et al.* Marine heatwaves threaten global biodiversity and the provision of ecosystem services. *Nat Clim Chang* **9**, 306–312 (2019).
7. Smith, K. E. *et al.* Biological Impacts of Marine Heatwaves. *Ann Rev Mar Sci* **15**, (2023).
8. Smith, K. E. *et al.* Socioeconomic impacts of marine heatwaves: Global issues and opportunities. *Science (1979)* **374**, 6566 (2021).
9. Oliver, E. C. J. *et al.* Marine Heatwaves. *Ann Rev Mar Sci* **13**, 313–342 (2021).
10. Benthuysen, J. A., Oliver, E. C. J., Feng, M. & Marshall, A. G. Extreme Marine Warming Across Tropical Australia During Austral Summer 2015–2016. *J Geophys Res Oceans* **123**, 1301–1326 (2018).
11. Elzahaby, Y. & Schaeffer, A. Observational Insight Into the Subsurface Anomalies of Marine Heatwaves. *Front Mar Sci* **6**, 745 (2019).
12. Elzahaby, Y., Schaeffer, A., Roughan, M. & Delaux, S. Oceanic Circulation Drives the Deepest and Longest Marine Heatwaves in the East Australian Current System. *Geophys Res Lett* **48**, e2021GL094785 (2021).
13. Scannell, H. A., Johnson, G. C., Thompson, L., Lyman, J. M. & Riser, S. C. Subsurface Evolution and Persistence of Marine Heatwaves in the Northeast Pacific. *Geophys Res Lett* **47**, e2020GL090548 (2020).
14. Ryan, S. *et al.* Depth Structure of Ningaloo Niño/Niña Events and Associated Drivers. *J Clim* **34**, 1767–1788 (2021).
15. Oliver, E. C. J. *et al.* Marine heatwaves off eastern Tasmania: Trends, interannual variability, and predictability. *Prog Oceanogr* **161**, 116–130 (2018).
16. Schaeffer, A. & Roughan, M. Subsurface intensification of marine heatwaves off southeastern Australia: The role of stratification and local winds. *Geophys Res Lett* **44**, 5025–5033 (2017).
17. Hu, S. *et al.* Observed strong subsurface marine heatwaves in the tropical western Pacific Ocean. *Environmental Research Letters* **16**, 104024 (2021).

18. Großelindemann, H., Ryan, S., Ummenhofer, C. C., Martin, T. & Biastoch, A. Marine Heatwaves and Their Depth Structures on the Northeast U.S. Continental Shelf. *Frontiers in Climate* **4**, 857937 (2022).
19. Jackson, J. M., Johnson, G. C., Dosser, H. v. & Ross, T. Warming From Recent Marine Heatwave Lingers in Deep British Columbia Fjord. *Geophys Res Lett* **45**, 9757–9764 (2018).
20. Holbrook, N. J. *et al.* Keeping pace with marine heatwaves. *Nat Rev Earth Environ* **1**, 482–493 (2020).
21. Global Monitoring and Forecasting Center. GLORYS12V1-Global Ocean Physical Reanalysis Product. *E.U. Copernicus Marine Service Information [Data set]. Available at: https://resources.marine.copernicus.eu/?option=com_csw&view=details&product_id=GLOBAL_REANALYSIS_PHY_001_030 (Accessed:13th May 2021)* (2018) doi:https://doi.org/10.48670/moi-00021.
22. Brito-Morales, I. *et al.* Climate velocity reveals increasing exposure of deep-ocean biodiversity to future warming. *Nat Clim Chang* **10**, 576–581 (2020).
23. Kaschner, K. *et al.* AquaMaps: Predicted range maps for aquatic species. Retrieved from https://www.aquamaps.org. http://www.marine.csiro.au/csquares/ (2019).
24. Jacox, M. G. *et al.* Impacts of the 2015–2016 El Niño on the California Current System: Early assessment and comparison to past events. *Geophys Res Lett* **43**, 7072–7080 (2016).
25. Hobday, A. J. *et al.* A hierarchical approach to defining marine heatwaves. *Prog Oceanogr* **141**, 227–238 (2016).
26. Holte, J., Talley, L. D., Gilson, J. & Roemmich, D. An Argo mixed layer climatology and database. *Geophys Res Lett* **44**, 5618–5626 (2017).
27. Imawaki, S., Zenk, W., Wijffels, S., Roemmich, D. & Masaki, K. Oceanic Boundary Currents. in *Observing the Oceans in the 21st Century* (eds. Koblinsky, C. & Smith, N.) (Godae Project Office, Bureau of Meteorology, 2001).
28. Chaikin, S., Dubiner, S. & Belmaker, J. Cold-water species deepen to escape warm water temperatures. *Global Ecology and Biogeography* **31**, 75–88 (2022).
29. Cartes, J. E., Maynou, F., Fanelli, E., López-Pérez, C. & Papiol, V. Changes in deep-sea fish and crustacean communities at 1000-2200m in the Western Mediterranean after 25years: Relation to hydro-climatic conditions. *Journal of Marine Systems* **143**, 138–153 (2015).
30. Polyakov, I. V. *et al.* Greater role for Atlantic inflows on sea-ice loss in the Eurasian Basin of the Arctic Ocean. *Science (1979)* **356**, 285–291 (2017).
31. Woodgate, R. A. Increases in the Pacific inflow to the Arctic from 1990 to 2015, and insights into seasonal trends and driving mechanisms from year-round Bering Strait mooring data. *Prog Oceanogr* **160**, 124–154 (2018).
32. Schmidtko, S., Heywood, K. J., Thompson, A. F. & Aoki, S. Multidecadal warming of Antarctic waters. *Science (1979)* **346**, 1227–1231 (2014).
33. Strass, V. H., Rohardt, G., Kanzow, T., Hoppema, M. & Boebel, O. Multidecadal warming and density loss in the Deep Weddell Sea, Antarctica. *J Clim* **33**, 9863–9881 (2020).
34. Holbrook, N. J. *et al.* A global assessment of marine heatwaves and their drivers. *Nat Commun* **10**, 2624 (2019).
35. sen Gupta, A. *et al.* Drivers and impacts of the most extreme marine heatwaves events. *Sci Rep* **10**, 19359 (2020).

36. Varela, R., Rodríguez-Díaz, L., de Castro, M. & Gómez-Gesteira, M. Influence of Eastern Upwelling systems on marine heatwaves occurrence. *Glob Planet Change* **196**, 103379 (2021).
37. Pinault, J. L. A Review of the Role of the Oceanic Rossby Waves in Climate Variability. *J Mar Sci Eng* **10**, 493 (2022).
38. Suryan, R. M. *et al.* Ecosystem response persists after a prolonged marine heatwave. *Sci Rep* **11**, 6235 (2021).
39. Wernberg, T. *et al.* Climate-driven regime shift of a temperate marine ecosystem. *Science (1979)* **353**, 169–172 (2016).
40. Straub, S. C. *et al.* Resistance, Extinction, and Everything in Between – The Diverse Responses of Seaweeds to Marine Heatwaves. *Front Mar Sci* **6**, 763 (2019).
41. Garrabou, J. *et al.* Collaborative Database to Track Mass Mortality Events in the Mediterranean Sea. *Front Mar Sci* **6**, 707 (2019).
42. Haguenauer, A. *et al.* Deep heat: A comparison of water temperature, anemone bleaching, anemonefish density and reproduction between shallow and mesophotic reefs. *Fishes* **6**, 37 (2021).
43. Bavestrello, G., Bo, M., Canese, S., Sandulli, R. & Cattaneo-Vietti, R. The red coral populations of the gulfs of Naples and Salerno: human impact and deep mass mortalities. *Italian Journal of Zoology* **81**, 552–563 (2014).
44. Perkins, N. R., Monk, J., Soler, G., Gallagher, P. & Barrett, N. S. Bleaching in sponges on temperate mesophotic reefs observed following marine heatwave events. *Climate Change Ecology* **3**, 100046 (2022).
45. Hughes, T. P. *et al.* Global warming and recurrent mass bleaching of corals. *Nature* **543**, 373–377 (2017).
46. Arafeh-Dalmau, N. *et al.* Extreme Marine Heatwaves alter kelp forest community near its equatorward distribution limit. *Front Mar Sci* **6**, 499 (2019).
47. Wernberg, T. Marine Heatwave Drives Collapse of Kelp Forests in Western Australia. in *Ecosystem Collapse and Climate Change* (eds. Canadell, J. G. & Jackson, R. B.) 325–343 (Springer Nature, 2021).
48. Santana-Falcón, Y. & Séférian, R. Climate change impacts the vertical structure of marine ecosystem thermal ranges. *Nat Clim Chang* **12**, 935-942 (2022).
49. Jorda, G. *et al.* Ocean warming compresses the three-dimensional habitat of marine life. *Nat Ecol Evol* **4**, 109–114 (2020).
50. Gouvêa, L. P. *et al.* Phenotypic Plasticity in Sargassum Forests May Not Counteract Projected Biomass Losses Along a Broad Latitudinal Gradient. *Ecosystems* **26**, 29-41(2022).
51. Schubert, N., Santos, R. & Silva, J. Living in a Fluctuating Environment Increases Tolerance to Marine Heatwaves in the Free-Living Coralline Alga Phymatolithon lusitanicum. *Front Mar Sci* **8**, 791422 (2021).
52. Coleman, M. A. & Wernberg, T. The Silver Lining of Extreme Events. *Trends Ecol Evol* **35**, 1065–1067 (2020).
53. Pershing, A. J., Mills, K. E., Dayton, A. M., Franklin, B. S. & Kennedy, B. T. Evidence for adaptation from the 2016 marine heatwave in the Northwest Atlantic Ocean. *Oceanography* **31**, 152–161 (2018).
54. Seuront, L., Nicastro, K. R., Zardi, G. I. & Goberville, E. Decreased thermal tolerance under recurrent heat stress conditions explains summer mass mortality of the blue mussel Mytilus edulis. *Sci Rep* **9**, 17498 (2019).
55. Dalton, S. J. *et al.* Successive marine heatwaves cause disproportionate coral bleaching during a fast phase transition from El Niño to La Niña. *Sci Total Environ* **715**, 136951(2020).

56. Rogers-Bennett, L. & Catton, C. A. Marine heat wave and multiple stressors tip bull kelp forest to sea urchin barrens. *Sci Rep* **9**, 15050 (2019).
57. Donovan, M. K. *et al.* Local conditions magnify coral loss after marine heatwaves. *Science (1979)* **372**, 977–980 (2021).
58. Danovaro, R., Dell'Anno, A. & Pusceddu, A. Biodiversity response to climate change in a warm deep sea. *Ecol Lett* **7**, 821–828 (2004).
59. Ashford, O. S. *et al.* Phylogenetic and functional evidence suggests that deep-ocean ecosystems are highly sensitive to environmental change and direct human disturbance. *Proc R Soc B: Biol Sci* **285**, 20180923 (2018).
60. Sweetman, A. K. *et al.* Major impacts of climate change on deep-sea benthic ecosystems. *Elementa: Sci Anthrop* **5**, 4 (2017).
61. Shi, Z., Assis, J. & Costello, M. J. Vulnerability of Marine Species to Low Oxygen Under Climate Change. in *Imperiled: The Encyclopedia of Conservation* (Elsevier, 2022).
62. IPCC 2021. *Climate Change 2021: The Physical Science Basis*. *Climate Change 2021: The Physical Science Basis. Contribution of Working Group I to the Sixth Assessment Report of the Intergovernmental Panel on Climate Change [Masson-Delmotte, V., P. Zhai, A. Pirani, S.L. Connors, C. Péan, S. Berger, N. Caud, Y. Chen,* (2021).
63. Gerringer, M. E. *et al.* Habitat influences skeletal morphology and density in the snailfishes (family Liparidae). *Front Zool* **18**, 16 (2021).

Methods

Daily global temperature data with depth covering 1993-2019

MHW characteristics were estimated using daily temperature timeseries derived from the Global Ocean Physics Reanalysis (GLORYS12V1)[21] provided by the E.U. Copernicus Marine Service (CMEMS). This is an eddy-permitting (1/12º) ocean reanalysis based on the NEMO ocean model. The model is forced by ERA-interim (between 1993 and 2018) and ERA5 surface fluxes subsequently and assimilates satellite altimetry, sea surface temperature and sea ice data as well as *in-situ* temperature and salinity profiles from the CORA[64] database, which has global coverage and includes ARGO program data (S1 Fig. 1). Temperature data are available at 50 depth levels covering the period 1993-2019.

The ability of the GLORYS12V1 reanalysis to capture ocean processes has been previously verified against *in-situ* observations and alternative models at local[65–67] and global[68] scales. However, some regional limitations exist. Specifically, the GLORYS12V1 shows a higher than observed warming trend[68] and temperature biases (up to 1.2°C) occurring in the

50-100 m depth in the Atlantic and 50-200 m depth in the Indian Ocean[69]. Because MHW estimates depend on temperature variability and not on mean temperature[25], we assessed the temporal variation of GLORYS12V1 against daily *in-situ* temperature datasets. Cross-validation was performed between daily *in-situ* records, at the available locations (geographical position, depth and date), and the nearest cell from the GLORYS12V1 reanalysis (as in[69,70]). The paired relationships were statistically compared based on the mean absolute error (MAE) of temperature, the mean absolute error of temperature variance from the mean (MAEvar), and Pearson's correlation. The cross-validation scheme was based on three different *in-situ* datasets (S1 Fig. 2): (1) the "polar moorings" timeseries dataset (independent data that have not been assimilated in the reanalysis model) consisted of 47 moorings from 13 sources (S1 Table 1), resulting in 1.09 million daily temperature records at different depths; (2) the "NOAA" timeseries dataset (assimilated in the reanalysis model) consisted of 70 TAO/TRITON moorings in the tropical Pacific and 20 PIRATA moorings in the Atlantic from the NOAA Pacific Marine Environmental Laboratory[71], covering the period from 1993 to 2019, and resulting in 7.6 million daily temperature records at different depths; (3) the Global Ocean Data Analysis Project (GLODAPv2.1) dataset[72] (independent data that have not been assimilated in the reanalysis model), derived by quality-controlled temperature observations from cruises across the global ocean, resulting in 680,777 records at different depths. Because the GLODAPv2.1 dataset does not provide temperature in timeseries, only spatial differences in temperature were assessed and not temporal variability.

Cross-correlations of the GLORYS12V1 against the polar moorings resulted in a MAE of 0.075°C, MAEvar of $1.4e^{-15}$ °C and a mean correlation across depths of 0.842 (S1 Table 2). The lowest correlations were estimated at 150-500 m depth, ranging from 0.459 to 0.601 and the largest MAE of 0.426°C between 0-25 m depth (S1 Table 2). Cross-correlations against the NOAA moorings resulted in a MAE of 0.101°C, MAEvar of $1.8e^{-15}$ °C and a mean correlation for all depths of 0.991 (S1 Table 2). The lowest correlation (0.858) was estimated at 500-1000 m depth and the larger MAE of 1.2°C between 200-250 m depth. Cross-correlations against the GLODAPv2.1 dataset resulted in a MAE of 0.049ºC and a mean correlation of 0.996 (S1 Table 2). The lowest correlation (0.983) was estimated at 500-1000 m depth and the larger MAE of 0.23ºC between 200-250 m depth. Examples of correlation plots of temperature variability between the GLORYS12V1 and the *in-situ* timeseries are presented in S1 Fig. 3 and S1 Fig. 4 and all plots are available in Figshare (https://doi.org/10.6084/m9.figshare.19174985). Also, scatterplots of the temperature correlation between the GLORYS12V1 and each of the three *in-situ* datasets are presented in S1 Fig. 5, S1 Fig. 6 and S1 Fig. 7. Lastly, the spatial distribution of temperature errors (S1 Fig. 8) for each depth was mapped onto a 2.5º grid by determining the average difference between the GLORYS12V1 and all three *in-situ* datasets[70]. Analyses revealed a spatial distribution of errors being larger between 50-250 m depth, reaching regionally up to 6ºC (S1 Fig. 8). However, temperature differences were mostly restricted to regions of the northwestern (in the extension of the Gulf Stream) and central Atlantic Ocean (S1 Fig. 8). Despite the regional temperature errors, correlations in temperature variability between the reanalysis and *in-situ* datasets were still high, therefore, not affecting the MHW estimates that depend on temperature variability and not on mean temperature.

Overall, we show that the GLORYS12V1 captures well temperature variability and can be used to estimate MHWs across the global ocean, despite the existing regional differences against the *in-situ* datasets. Yet, it is important to acknowledge that the reanalysis may still carry biases that influence the prediction of extreme events, especially in regions/depths where lower correlations were found. Specifically in polar regions, where the lowest correlations between the reanalysis and *in-situ* datasets were found, MHW estimates have higher uncertainty, due to the reduced number of *in-situ* data feeding the model.

Spatial and depth resolution of global MHW estimates

The GLORYS12V1 dataset was re-gridded onto an equal-area 60 km-resolution hexagon grid (approx. 0.5° resolution) using Uber's standardized hexagonal hierarchical spatial data griding system[73]. Mean daily temperatures were retrieved for each hexagon to produce distinct baseline climatologies for the identification of MHW events at eleven depths: 0, 25, 50, 75, 100, 150, 200, 250, 500, 1000 and 2000 m. Uber's hexagonal framework was chosen due to its equal-area projection and optimal indexing algorithm, which allows fast data aggregation over its hierarchical resolutions[73].

MHW analyses and characteristics with depth

Marine heatwave events were identified following the definition of Hobday[25], which defines a MHW as a discrete prolonged anomalously warm water event of at least 5-day duration, during which daily temperatures exceeded the 90th percentile threshold of the historical baseline climatology (in our case 27 years, from 1993 to 2019). Events less than 3 days apart were considered a single event. The historical baseline climatology for a given day was calculated using an 11-day window centred on that date across all years of the climatology period, and an additional 31-day moving average was applied to smooth the climatology[25]. A daily varying threshold was preferred to an absolute fixed value, as it allowed the identification of MHW events throughout the year, rather than during the warmest seasons only. Each MHW event was characterized by a set of metrics[25], namely the duration (days), maximum intensity (°C), cumulative intensity (°C days) and the absolute temperature (°C) of the ocean at the peak of maximum intensity. Metrics were estimated independently for each depth. Regional (hexagon) estimates were calculated as the average of each metric for the years 1993-2019.

Regional MHW occurrence was calculated as the total number of events from 1993-2019 in each hexagon. Global estimates per depth were calculated as the average of all hexagons for each depth. Regional time-depth MHW and biodiversity (see below) metrics (i.e., MHW maximum intensity, cumulative intensity, temperature profiles, species richness and warm-edge richness) were calculated as the daily average of hexagons at a 2 by 2-degree resolution for each depth.

To explore potential temporal synchrony between the warming of the surface and subsurface layers, Pearson's correlation coefficients for temperature anomalies were determined and p-values were estimated as a measure of statistical significance ($p < 0.05$) using the package "synchrony"[74] which accounts for temporal autocorrelation.

Biodiversity data

We used species richness as an indicator of biodiversity. Richness was estimated from 25,078 modelled marine species ranges available in AquaMaps[23], including fishes, invertebrates, mammals, algae and seagrasses. AquaMaps produces standardized species distribution maps using a probability of occurrence threshold (0-1) resulting from environmental niche models at 0.5° resolution. Here, we used a minimum threshold of 0.5 probability of occurrence to define species ranges[22,75]. Considering the depth preferences of each species provided by the AquaMaps database, we categorized their distributions on the depth layers for which MHWs were estimated. Species richness was estimated as the number of species with distribution ranges within each hexagon grid (approx. 0.5° resolution. Because populations at the warm range edge of their distribution are more likely to exceed their thermal tolerance when exposed to MHWs[6], we inferred temperature-sensitive populations for each species by dividing their distribution into terciles, corresponding to the cold, central and warm distribution range edge[6], based on the average temperature from 1993-2019 (derived from the same daily data used to estimate MHWs). Warm-edge richness was determined as the number of species at their warm range edge within each hexagon. Estimates of species richness, warm-edge richness and cumulative intensity at a given depth were divided into terciles, corresponding to low, medium and high values[22], and hexagons were reclassified accordingly. We estimated potential richness/warm-edge exposure as the overlap of MHW cumulative intensity (as a measure of cumulative heat stress on biodiversity[76,77]) and species richness/warm-edge richness per hexagon. Nine exposure categories were defined as the overlap of tercile combinations between cumulative intensity and biodiversity metrics. The highest exposure was considered in cells where high cumulative intensity overlapped high species richness/warm-edge richness. In contrast, the lowest exposure was considered in cells where low cumulative intensity overlapped high species richness/ warm-edge richness.

All analyses were conducted in R[78] and the code is openly available in Figshare[79]. MHWs were estimated using the package "RmarineHeatWaves" and thermocline depth was estimated using the function "thermo.depth" of the "rLAkeAnalyser". Individual global maps depicting MHW and biodiversity metrics can be found in Figshare (https://doi.org/10.6084/m9.figshare.19174985).

Data availability

Daily temperature reanalysis data (GLORYS12V1) are openly provided by the E.U. Copernicus Marine Service (https://doi.org/10.48670/moi-00021). The biodiversity dataset is openly available from Aquamaps at https://www.aquamaps.org. The datasets used for the validation of the GLORYS12V1 reanalysis are: (1) the NOAA dataset (https://doi.org/10.5270/OceanObs09.cwp.61), available for download at: https://www.pmel.noaa.gov/tao/drupal/disdel/, and (2) the GLODAPv2 dataset (https://doi.org/10.5194/essd-13-5565-2021) available for download at: https://www.glodap.info/index.php/merged-and-adjusted-data-product-v22021/. Sources and detailed information on the (3) "polar moorings" dataset can be found in Supplementary Material 1 Table 1.

Code availability

R code for data collection and MHW analyses is openly available on Figshare (https://doi.org/10.6084/m9.figshare.19174985).

Methods references

64. Szekely, T., Gourrion, J., Pouliquen, S. & Reverdin, G. CORA, Coriolis Ocean Dataset for Reanalysis. *SEANOE* (2023) https://doi.org/10.17882/46219.
65. Verezemskaya, P. *et al.* Assessing Eddying (1/12°) Ocean Reanalysis GLORYS12 Using the 14-yr Instrumental Record From 59.5°N Section in the Atlantic. *J Geophys Res Oceans* **126**, e2020JC016317 (2021).
66. Artana, C. *et al.* The Malvinas Current at the Confluence With the Brazil Current: Inferences From 25 Years of Mercator Ocean Reanalysis. *J Geophys Res Oceans* **124**, 7178–7200 (2019).
67. Poli, L. *et al.* Anatomy of Subinertial Waves Along the Patagonian Shelf Break in a 1/12° Global Operational Model. *J Geophys Res Oceans* **125**, e2020JC016549 (2020).
68. Lellouche, J.-M. *et al.* The Copernicus Global 1/12° Oceanic and Sea Ice GLORYS12 Reanalysis. *Front Earth Sci* **9**, 698876 (2021).
69. Drévillon, M. *et al. Quality information document for Global Ocean Reanalysis Products GLOBAL_REANALYSIS_PHY_001_030*. https://catalogue.marine.copernicus.eu/documents/QUID/CMEMS-GLO-QUID-001-030.pdf (2021) https://doi.org/10.48670/moi-00021.
70. Assis, J. *et al.* Bio-ORACLE v2.0: Extending marine data layers for bioclimatic modelling. *Global Ecology and Biogeography* **27**, 277–284 (2018).
71. McPhaden, M. J. *et al.* The Global Tropical Moored Buoy Array. in *Proceedings of OceanObs'09: Sustained Ocean Observations and Information for Society* 668–682 (European Space Agency, 2010). doi:10.5270/OceanObs09.cwp.61.
72. Olsen, A. *et al.* The global ocean data analysis project version 2 (GLODAPv2) - An internally consistent data product for the world ocean. *Earth Syst Sci Data* **8**, 297–323 (2016).
73. Bondaruk, B., Roberts, S. A. & Robertson, C. Assessing the state of the art in Discrete Global Grid Systems: OGC criteria and present functionality. *Geomatica* **74**, 9–30 (2020).
74. Gouhier, T. C. & Guichard, F. Synchrony: Quantifying variability in space and time. *Methods Ecol Evol* **5**, 524–533 (2014).
75. Klein, C. J. *et al.* Shortfalls in the global protected area network at representing marine biodiversity. *Sci Rep* **5**, 17539 (2015).
76. Laufkötter, C., Zscheischler, J. & Frölicher, T. L. High-impact marine heatwaves attributable to human-induced global warming. *Science (1979)* **369**, 1621–1625 (2020).
77. Wyatt, A. S. J. *et al.* Hidden heatwaves and severe coral bleaching linked to mesoscale eddies and thermocline dynamics. *Nat Commun* **14**, 25 (2023).
78. R Core Team. (2021) R: A language and environment for statistical computing. R Foundation for Statistical Computing, Vienna, Austria. URL https://www.R-project.org.
79. Fragkopoulou et al., Marine biodiversity exposed to prolonged and intense subsurface heatwaves. figshare. Journal Contribution. (2023) https://doi.org/10.6084/m9.figshare.19174985